ORIGINAL RESEARCH

Gastrin-releasing peptide receptor-targeted gadolinium oxide-based multifunctional nanoparticles for dual magnetic resonance/ fluorescent molecular imaging of prostate cancer

Danting Cui[1]
Xiaodan Lu[1]
Chenggong Yan[1]
Xiang Liu[1]
Meirong Hou[1]
Qi Xia[2]
Yikai Xu[1]
Ruiyuan Liu[2,3]

[1]Department of Medical Imaging Center, Nanfang Hospital, Southern Medical University, Guangzhou, People's Republic of China; [2]School of Pharmaceutical Sciences, Southern Medical University, Guangzhou, People's Republic of China; [3]School of Biomedical Engineering, Southern Medical University, Guangzhou, People's Republic of China

Correspondence: Yikai Xu
Department of Medical Imaging Center, Nanfang Hospital, Southern Medical University, Guangzhou 510515, Guangdong, People's Republic of China
Tel/fax +86 20 6278 7333
Email yikaixu917@gmail.com

Ruiyuan Liu
School of Biomedical Engineering, Southern Medical University, Guangzhou 510515, Guangdong, People's Republic of China
Tel/fax +86 20 6164 8196
Email ruiyliu@smu.edu.cn

Abstract: Bombesin (BBN), an analog of gastrin-releasing peptide (GRP), specifically binds to GRP receptors, which are overexpressed in human prostate cancer (PC). Here, we synthesized a BBN-modified gadolinium oxide (Gd_2O_3) nanoprobe containing fluorescein (Gd_2O_3-5(6)-carboxyfluorescein [FI]-polyethylene glycol [PEG]-BBN) for targeted magnetic resonance (MR)/optical dual-modality imaging of PC. The Gd_2O_3-FI-PEG-BBN nanoparticles exhibited a relatively uniform particle size with an average diameter of 52.3 nm and spherical morphology as depicted by transmission electron microscopy. The longitudinal relaxivity (r_1) of Gd_2O_3-FI-PEG-BBN (r_1 =4.23 $mM^{-1}s^{-1}$) is comparable to that of clinically used Magnevist (Gd-DTPA). Fluorescence microscopy and in vitro cellular MRI demonstrated GRP receptor-specific and enhanced cellular uptake of the Gd_2O_3-FI-PEG-BBN in PC-3 tumor cells. Moreover, Gd_2O_3-FI-PEG-BBN showed more remarkable contrast enhancement than the corresponding nontargeted Gd_2O_3-FI-PEG according to in vivo MRI and fluorescent imaging. Tumor immuno-histochemical analysis further demonstrated improved accumulation of the targeted nanoprobe in tumors. BBN-conjugated Gd_2O_3 may be a promising nanoplatform for simultaneous GRP receptor-targeted molecular cancer diagnosis and antitumor drug delivery in future clinical applications.

Keywords: magnetic resonance imaging, gadolinium oxide, bombesin, gastrin-releasing peptide receptor, molecular imaging

Introduction

Prostate cancer (PC) is one of the leading causes of cancer-related deaths worldwide.[1] Because of its asymptomatic and multifocal nature, it has been challenging to accurately detect cancer lesions in early stages.[2] Conventional imaging, which includes magnetic resonance imaging (MRI), computed tomography, and transrectal ultrasound, is routinely used for PC staging and prognostic determination.[3] However, there is substantial room for improvement in the specificity and sensitivity of imaging for early staged PC.

Gastrin-releasing peptide receptors (GRPRs) are attractive targets for sensitive molecular imaging, as they are overexpressed in human PC.[4] Bombesin (BBN)-based peptides show high binding affinity to GRPRs and could be exploited as specific tumor-targeting ligands.[5] Previous studies have employed several radiolabeled BBN derivatives for GRPR-positive tumor diagnostics and treatment with high efficacy.[6–8] However, radionuclide imaging suffers from long scan time and ionizing radiation. Recently, some progress has been made in tumor-targeted MR/optical dual-modality

imaging.[9] MRI offers several advantages including high anatomical resolution and a lack of harmful radiation. Furthermore, real-time optical imaging is used for intraoperative guidance during surgery. Hence, the design and development of new BBN-based conjugates may provide noninvasive imaging strategies for the detection and localization of GRPR expression in vivo.

Currently, gadolinium oxide (Gd_2O_3) nanoparticles (NPs) have been investigated for MR molecular imaging.[10] These NPs can provide high longitudinal relaxivities that are equal to or even larger than clinically approved Gd-DTPA allowing more efficient contrast enhancement.[11] Moreover, Gd_2O_3 NPs offer a versatile platform for further multifunctionalization through modifications, which makes them good candidates for active tumor targeting and multimodal imaging.[12]

In this study, we report the development of a 5(6)-carboxyfluorescein (FI)-conjugated Gd_2O_3 nanoprobe for PC cell-specific targeted molecular imaging. Gd_2O_3 NPs were synthesized via a simple polyol-free synthesis at room temperature. The long hydrophilic polyethylene glycol (PEG) segments bearing BBN ligand facilitated specific binding to the overexpressed GRPR, which increased tumor selectivity.[13] Then, the physicochemical properties and cytotoxicity of Gd_2O_3-based nanoprobes were investigated. Cellular uptake efficiency was evaluated by fluorescence microscopy, flow cytometry and in vitro MRI. In vivo MR/optical dual-modality imaging was performed to monitor signal enhancement in the tumors of mice bearing GRPR-positive PC-3 xenografts.

Materials and methods
Materials and general methods
Gadolinium(III) acetate, dimethyl sulfoxide (DMSO), tetramethylammonium hydroxide (TMAH), anhydrous EtOH, FI, dichloromethane (DCM), α-carboxyl, ω-hydroxy PEG (PEG-2000), *N*-hydroxysuccinimide and 1-[3-(dimethylamino) propyl]-3-ethylcarbodiimide hydrochloride (EDC·HCl) were purchased from Adamas Chemical Reagents Co, Ltd (Shanghai, People's Republic of China). BBN, CGGG-QWAVGHLM-NH2(7–14), was synthesized using standard fluorenylmethoxycarbonyl (fmoc) chemistry solid phase peptide synthesis method by Boxin Biotechnology (Xiamen, People's Republic of China). All other chemicals were used without further purification.

Synthesis and sample preparations
Synthesis of the Gd_2O_3 NPs
The Gd_2O_3 NPs were synthesized according to previously published methods with little modification.[14] Briefly, Gd (OAc)$_3$ (670 mg, 2 mmol) was dissolved in DMSO (30 mL). Then, TMAH (200 mg, 5.6 mmol) in EtOH (10 mL) was added dropwise. After the total amount of TMAH was added, the mixture was stirred for 2 h at room temperature. The Gd_2O_3 NPs were collected by centrifugation. The particles were washed thoroughly by three cycles of centrifugation/redispersion in EtOH and vacuum concentrated to give Gd_2O_3 (630 mg, 87%).

Synthesis of Gd_2O_3-FI NPs
Gd_2O_3 (400 mg) dispersed in DMSO was reacted with 100 mg FI, under constant stirring for 12 h at room temperature. Gd_2O_3 NPs were capped with a fluorescent glycol-based conjugated carboxylate (H-L) which allowed L coordinated to the surface of Gd_2O_3 NPs effectively through the terminal carboxyl group. The product was purified by centrifugation and then washed three times with DMSO, EtOH and DCM sequentially. The pure product was dispersed in deionized (DI) water and freeze-dried to give Gd_2O_3-FI NPs (415 mg, 83%).

Synthesis of Gd_2O_3-FI-PEG NPs
Gd_2O_3-FI NPs (200 mg) were mixed with 100 mg PEG-2000 (dissolved in 10 mL DMSO) and reacted at room temperature under constant stirring for 12 h. PEG ligand was coordinated with Gd_2O_3 with terminal carboxyl group. The Gd_2O_3-FI-PEG NPs were collected by centrifugation and then washed three times with DMSO, EtOH and DCM sequentially. Then, Gd_2O_3-FI-PEG NPs were obtained to remove impurities. The NPs were added to DI water and freeze-dried to give Gd_2O_3-FI-PEG NPs (228 mg, 76%).

Synthesis of fluorescent GRPR-targeted Gd_2O_3 (Gd_2O_3-FI-PEG-BBN) NPs
BBN (20 mg), EDC·HCl (20 mg) and *N*-hydroxysuccinimide (10 mg) were mixed with 100 mg Gd_2O_3-FI-PEG that was dispersed in DMSO. The mixture was stirred for 12 h at room temperature and then centrifuged. Precipitates were collected by centrifugation and washed with DMSO, EtOH and DCM three times, respectively. The precipitate was dispersed in DI water and freeze-dried to give Gd_2O_3-FI-PEG-BBN (86 mg, 72%).

Physicochemical characterization
The particle size and morphology of the developed NPs were observed using transmission electron microscopy (TEM) (H-7650; HITACHI, Tokyo, Japan) operating at 200 kV. The hydrodynamic size distribution of the particles was

determined using dynamic light scattering (DLS) (Malvern Zeta-sizer 3000HS; Malvern Instruments, Malvern, UK) using a 633 nm laser. Thermal gravimetric analysis (TGA) was performed on a STA 209 F1 Iris instrument (Netzsch, Selb, Germany). The temperature was increased to 710°C at a rate of 10°C min^{-1} (in 100 mL min^{-1} helium flux). Fourier transform infrared (FTIR) spectra were recorded on a Vector 33 FTIR spectrophotometer (Bruker, Mannheim, Germany) using KBr pellets in the range 4,000–400 cm^{-1}. The Gd elemental content was determined by inductively coupled plasma atomic emission spectrometry.

Magnetic property measurements

NPs were prepared in 0, 0.25, 0.5, 1, 2, and 4 mmol/L Gd concentrations. Longitudinal relaxivities (r_1) of these suspensions were measured using a 3.0T MR system (Achieva TX; Philips Healthcare, Amsterdam, the Netherlands) equipped with an eight-channel head coil at room temperature. T1 relaxation times for each sample were obtained using T1-weighted spin-echo sequences by varying repetition times (TR =100, 200, 400, 600, and 1,000 ms) with fixed echo time (TE) =10 ms, and imaging parameters of slice thickness of 5 mm. The signal intensity of the samples was measured by defining regions of interest in the center of each test tube, and the T1 values were calculated accordingly using workstation software. The r_1 values were calculated from the slopes of the linear fitting of 1/T1 (s^{-1}) versus the Gd concentration (mM).

In vitro cellular studies

Cell culture

The PC-3 cancer cell lines (GRPR positive) were gifted from the Research Center of Clinical Medicine at Nanfang Hospital (Guangzhou, People's Republic of China). PC-3 cells were grown in Dulbecco's Modified Eagle's Medium (DMEM) supplemented with 10% fetal bovine serum, penicillin (100 U/mL) and streptomycin (100 U/mL) in a humidified incubator at 37°C with 5% CO_2.

Cytotoxicity assays

PC-3 cells were seeded in a 96-well plate at a density of 3,000 cells/well and cultured for 24 h. The culture medium was replaced with 200 µL DMEM containing Gd_2O_3-FI-PEG-BBN or control Gd_2O_3-FI-PEG at different concentrations (0.125, 0.25, 0.5, 1, 2, 4 and 8 mM Gd) and kept incubated for 24 or 48 h. Subsequently, 20 µL of MTT solution (5 mg/mL) was added and incubated for 4 h before the addition of 150 µL of DMSO into each well to dissolve the formazan crystals. Complete dissolution was achieved by shaking on

tabletop oscillator for 10 min. The absorbance of each well was measured at 490 nm using a BIOTEK ELX80 enzyme-linked immunosorbent assay reader (Winooski, VT, USA). The control group contained cells and cell culture medium without NPs.

Analysis of intracellular uptake by fluorescence microscopy

PC-3 cells were seeded in six-well culture plates at a density of 4×10^5 cells/well and incubated for 24 h. The medium was then removed and replaced with 2 mL DMEM containing Gd_2O_3-FI-PEG-BBN or Gd_2O_3-FI-PEG suspensions (0.8 mM Gd). After incubation at 37°C for 4 h, the cells were washed three times with PBS and fixed with 2 mL 4% paraformaldehyde in PBS for 20 min. Cell nuclei were then stained with 4′,6-diamidino-2-phenylindole (DAPI). Cellular uptake was observed using a fluorescence microscope (Olympus BX51; Olympus Corporation, Tokyo, Japan).

Cellular uptake measured by flow cytometry

PC-3 cells were seeded in six-well plates at a density of 4×10^5 cells per well and incubated for 24 h. Gd_2O_3-FI-PEG-BBN or Gd_2O_3-FI-PEG NPs (0.8 mM Gd) were added to the wells and incubated for 4 h. The cells were harvested, and fluorescence was measured using a BD LSRII flow cytometer (BD Biosciences, San Jose, CA, USA).

In vitro cellular MRI

PC-3 cells were grown in DMEM containing both NPs (0.8 mM Gd) for 4 h, and labeled cells were washed with PBS and resuspended in 100 µL of DMEM and 1% agarose in Eppendorf tubes. The tubes were imaged on a 3.0T MR system with a routine T1-weighted FSE sequence. Parameters were as follows: TR/TE =500/10 ms, field of view =100×100×60 mm, matrix =256×256, number of excitation =2 and thickness/interval =4/0.5 mm.

Animal experiments and in vivo imaging

Tumor model

Animal experiments were approved by the Institutional Animal Care and Use Committee of Southern Medical University (Guangzhou, People's Republic of China) and performed in accordance with the institutional guidelines. Animals were cared for according to the Chinese National Guidelines for Animal Welfare. For tumor xenografts, a mixture of 6×10^6 PC-3 cells suspended in 0.15 mL PBS was injected subcutaneously into the left posterior foreleg region of male BALB/c-nude mice (4–5 weeks old). When

the average tumor diameter reached 1.0 cm (4–6 weeks after implantation), the mice were randomized into two groups: targeted Gd_2O_3-FI-PEG-BBN and non-targeted Gd_2O_3-FI-PEG, and prepared for further imaging.

In vivo MRI

Serial MRI was performed on a 3.0T MR system (Achieva TX; Philips Healthcare, the Netherlands) equipped with a mouse-imaging coil before and at different time points after injecting Gd_2O_3-FI-PEG-BBN or Gd_2O_3-FI-PEG (3 μmol Gd in 0.2 mL, n=5 per group). Coronal T1-weighted fast spin echo (FSE) (TR/TE =500/10 ms, field of view =100×100×17 mm, matrix =320×224, number of excitation =3 and thickness =2.0 mm) images were obtained. Pseudo-colored MRI images were processed with ImageJ software. To estimate the contrast enhancement of NPs in the tumor region, changes in the relative signal intensity were quantified based on the regions of interest.

In vivo near-infrared fluorescent imaging

To compare the targeting ability of Gd_2O_3-FI-PEG-BBN and Gd_2O_3-FI-PEG, fluorescent imaging was performed on PC-3 tumor-bearing mice (n=3 per group) using a Berthold NightOWL LB 983 in vivo imaging system (Bad Wildbad, Germany). The excitation filter was set at 530 nm, and the emission filter was set at 700 nm. Fluorescence images were obtained using a cooled charge-coupled device camera with constant exposure time and taken before and 2 h after intravenous injection of NPs.

Biodistribution

To study the tissue distribution of Gd_2O_3-FI-PEG-BBN, mice were sacrificed, the major organs (heart, liver, spleen, lung, kidneys and testis) were surgically removed 2 h postinjection, washed with PBS and imaged by IVIS® Spectrum (PerkinElmer Inc., Waltham, MA, USA) to calculate the average fluorescence intensities within tissues.

Histological analysis

After in vivo imaging, tumor tissues were collected and embedded in optimal cutting temperature compound. Frozen tumor tissue slices (5 μm) were stained with the fluorescent dye DAPI, and images were taken using a fluorescence microscope.

Statistical analysis

Statistical analysis was performed using a two-tailed unpaired Student's t-test with $P<0.05$ used as the cutoff value for significance. All values are presented as mean ± standard deviation (SD). All analyses were performed using SPSS 13.0 (SPSS Inc., Chicago, IL, USA).

Results and discussion

The preparation method of Gd_2O_3-FI-PEG-BBN was taken from existing literature with slight modifications (Figure 1).[14] The initial Gd_2O_3 NPs were prepared by alkaline hydrolysis of $Gd(OAC)_3$ in aqueous TMAH at room temperature. To improve the biocompatibility and water solubility of Gd_2O_3 NPs, the PEGylation strategy was adopted.[15] The Gd_2O_3 NPs then were capped with FI and PEG-2000 in DCM at room temperature to obtain Gd_2O_3-FI-PEG, which ensure a biocompatible and stable system and facilitate further modification.

Physicochemical characterization

TEM was used to investigate the morphology of the developed NPs. Figure 2A shows that Gd_2O_3-FI-PEG-BBN NPs were almost spherical and had a uniform size with an average diameter of 52.3 nm. The coating layer was visible in TEM images with negative staining. The hydrodynamic diameter of the targeted nanoprobe was 90.6 nm with a polydispersity index of 0.28, as measured by DLS (Figure 2B). The difference in size measurements can be attributed to the fact that TEM and DLS showed different morphologies in the solid and swollen states.[16]

Surface coating and functionalization of the samples were investigated by recording the FTIR spectrum. The FTIR spectrum for Gd_2O_3 was compared with that of Gd_2O_3-FI-PEG-BBN in Figure 2C. After coating Gd_2O_3 with PEG and FI, the observed absorption frequencies characteristic of PEG in Gd_2O_3-FI-PEG-BBN included the C–O stretch at 1,587 and 1,114 cm^{-1}, and the CH_2 stretch at 2,920 and 2,856 cm^{-1}. Furthermore, the C=O stretch at 1,716 cm^{-1} was prominent in HO-PEG-COOH and FI but disappeared in Gd_2O_3-FI-PEG-BBN, which is consistent with NPs coated by various carboxylic acids.[11] These data implied that PEG and FI were effectively coordinated to the surface of Gd_2O_3 through the terminal carboxyl group. Further modification by BBN led to a new peak at 1,595 cm^{-1} corresponding to amide bond formation.

TGA was used to determine the mass drop in weight (%) of the materials (Figure 2D). The weight loss of both developed NPs was ~20% due to the thermal decomposition of FI at around 30°C–100°C in air. Both nanoprobes showed significant weight loss because low molecular weight PEG degrades at 280°C. The mass loss of Gd_2O_3-FI-PEG-BBN and Gd_2O_3-FI-PEG produced at 700°C were 51% and 44%, respectively. Therefore, the extra mass drop of
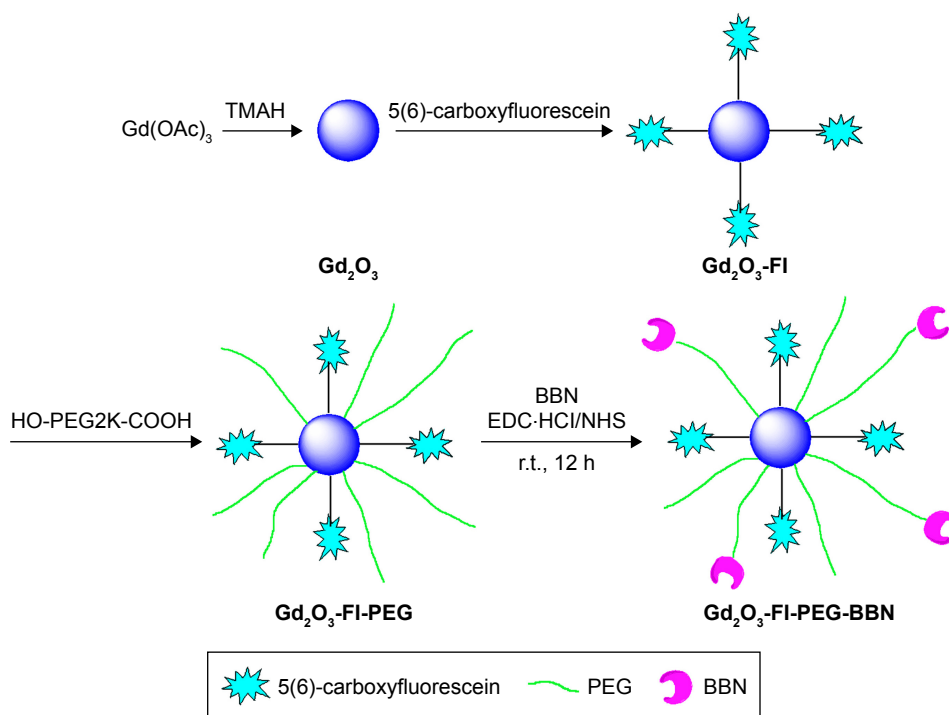
Figure 1 Schematic illustration of the synthesis of Gd$_2$O$_3$-Fl-PEG-BBN.
Abbreviations: BBN, bombesin; EDC·HCl, 1-[3-(dimethylamino)propyl]-3-ethylcarbodiimide hydrochloride; Fl, 5(6)-carboxyfluorescein; Gd$_2$O$_3$, gadolinium oxide; NHS, N-hydroxysuccinimide; PEG, polyethylene glycol; r.t., room temperature; TMAH, tetramethylammonium hydroxide.
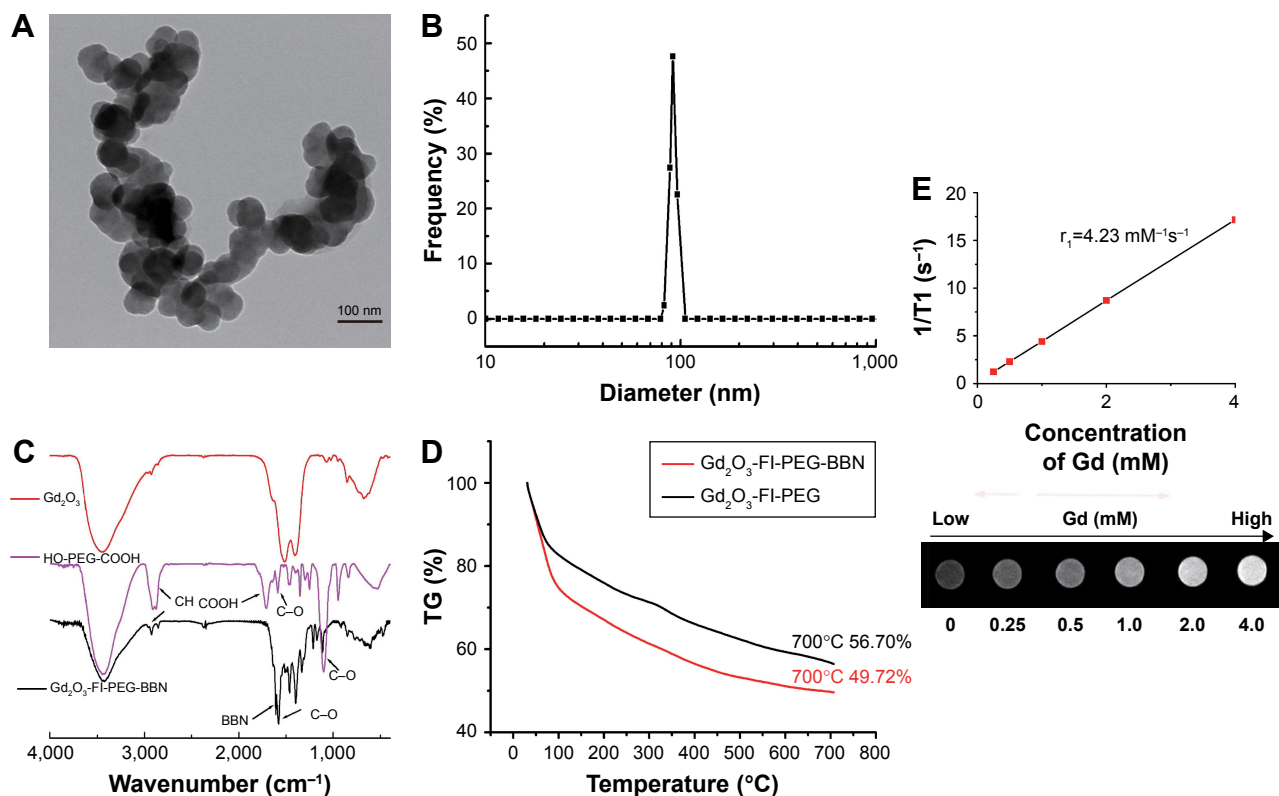
Figure 2 Characterization of nanoparticles.
Notes: TEM micrograph (**A**) and hydrodynamic size distribution (**B**) of Gd$_2$O$_3$-Fl-PEG-BBN. FTIR spectra (**C**) of uncoated Gd$_2$O$_3$ and Gd$_2$O$_3$-Fl-PEG-BBN. TGA curves (**D**) of Gd$_2$O$_3$-Fl-PEG and Gd$_2$O$_3$-Fl-PEG-BBN. T1-weighted turbo spin-echo (TSE) MR images and longitudinal relaxation r$_1$ (**E**) of Gd$_2$O$_3$-Fl-PEG-BBN solutions with various Gd concentrations.
Abbreviations: BBN, bombesin; Fl, 5(6)-carboxyfluorescein; FTIR, Fourier transform infrared spectroscopy; Gd$_2$O$_3$, gadolinium oxide; MR, magnetic resonance; PEG, polyethylene glycol; TEM, transmission electron microscopy; TGA, thermal gravimetric analysis.

Gd_2O_3-FI-PEG-BBN (7%) corresponded to the decomposition of the BBN coating.

Magnetic property measurements

The ability of contrast agent to alter T1 was assessed via longitudinal relaxivity (r_1). The T1-weighted MR images (Figure 2E) revealed that MR signals of Gd_2O_3-FI-PEG-BBN enhanced as the Gd concentrations increased. As indicated by the slope of the fitting line shown in Figure 2E, the calculated r_1 value of Gd_2O_3-FI-PEG-BBN was 4.23 mM^{-1}s^{-1}, which was comparable to that of Magnevist (4.29 mM^{-1}s^{-1}) reported previously.[17] The relatively high r_1 of Gd_2O_3-FI-PEG-BBN could be due to the polar C=O group increasing the number of exchangeable water molecules in the inner sphere of the Gd^{3+} ions, which is known to be directly related to contrast enhancing capacity.[18] This suggests that Gd_2O_3-FI-PEG-BBN can serve as a highly efficient T1-weighted MRI contrast agent.

Cytotoxicity assay

The in vitro cytotoxicity of Gd_2O_3-FI-PEG and Gd_2O_3-FI-PEG-BBN was evaluated by MTT viability assays. Figure 3 shows the viability of PC-3 cells incubated with both NPs at various Gd concentrations (0–8 mM). Even at 8 mM Gd, the cell viability remained 112.9%±3.6% after 24 h and 110.2%±6.8% after 48 h incubation with Gd_2O_3-FI-PEG-BBN. Similarly, no significant cell viability reduction was observed for Gd_2O_3-FI-PEG. In accordance to other published

data,[19,20] Gd_2O_3-based NPs did not present any cytotoxic activity. These results indicated that Gd_2O_3-FI-PEG and Gd_2O_3-FI-PEG-BBN are relatively biocompatible and have low toxicity at this Gd concentration range.

Specificity of targeting PC-3 cells in vitro

To investigate the targeting efficacy and intracellular distribution of the developed probes, we incubated the Gd_2O_3 nanoprobe with GRPR-positive PC-3 cells. The green fluorescence of FI was used for the observation of GRPR-mediated intracellular delivery. As shown in Figure 4A, green fluorescence was clearly observed in PC-3 cells treated with Gd_2O_3-FI-PEG-BBN. However, only weak green fluorescence was detected in cells incubated with Gd_2O_3-FI-PEG. This was attributed to the fact that BBN can remarkably enhance NPs uptake through GRPR-mediated endocytosis.[21] Moreover, fluorescence microscopy images showed that Gd_2O_3-FI-PEG-BBN fluorescence was predominantly accumulated in the cytoplasm around the nucleus.

Cellular uptake by flow cytometry

The uptake of Gd_2O_3-FI-PEG-BBN in PC-3 cells was also studied by flow cytometry. As shown in Figure 4B, cells incubated with Gd_2O_3-FI-PEG-BBN NPs showed much higher fluorescence intensity than those incubated with Gd_2O_3-FI-PEG and the blank cells. The area under each curve was proportional to the total number of fluorescent cells and was ~7.4-fold higher in Gd_2O_3-FI-PEG-BBN than in non-targeted
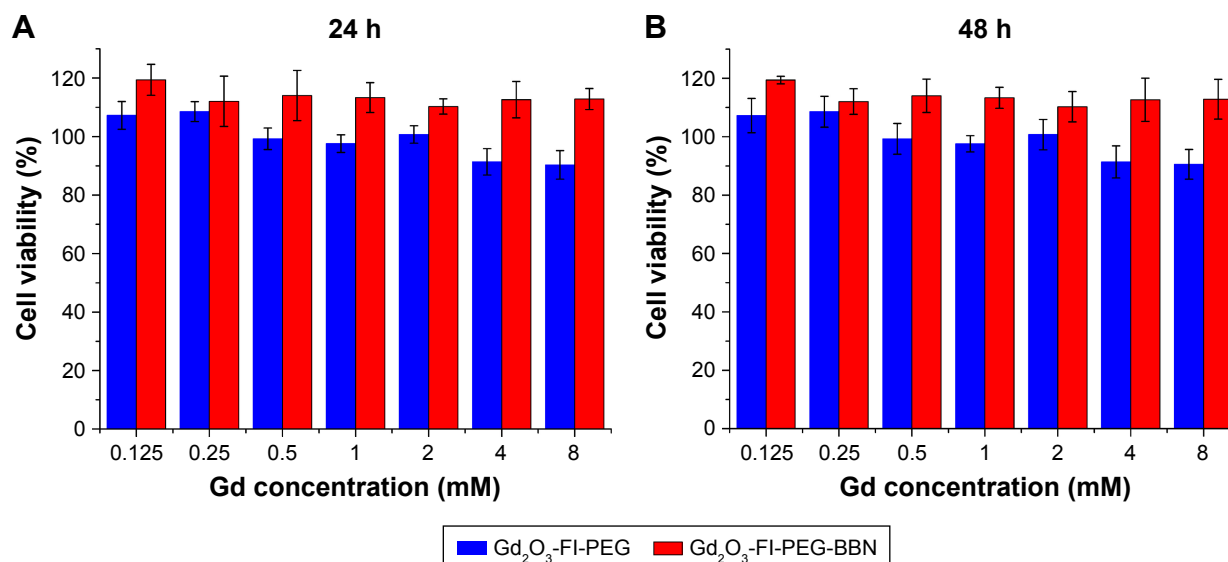
Figure 3 Cell viability assays of PC-3 cells treated with various concentrations of Gd_2O_3-FI-PEG-BBN or Gd_2O_3-FI-PEG for 24 (**A**) or 48 h (**B**).
Abbreviations: BBN, bombesin; FI, 5(6)-carboxyfluorescein; Gd_2O_3, gadolinium oxide; PEG, polyethylene glycol.
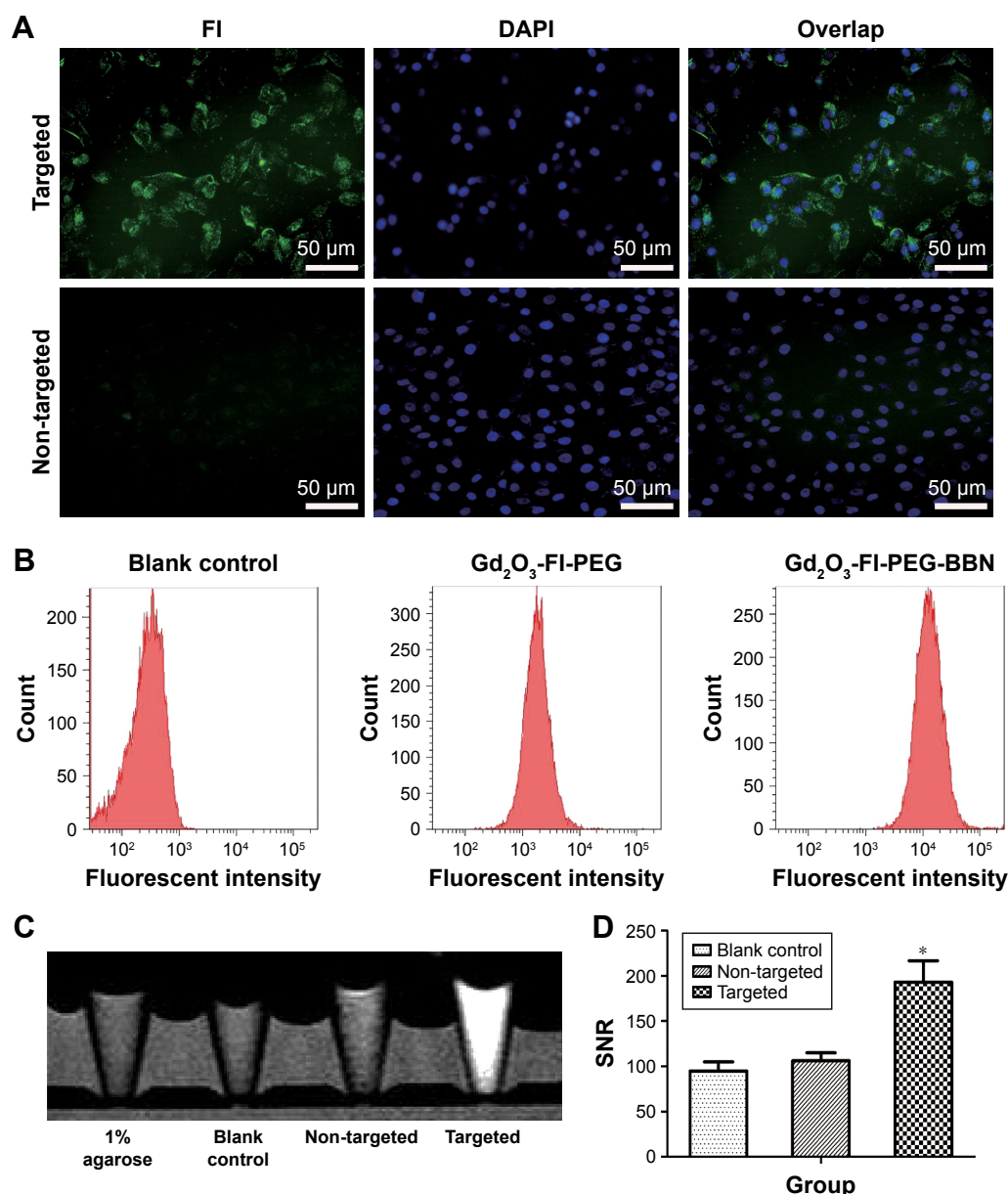
Figure 4 Fluorescence microscopy images (**A**), flow cytometry (**B**), T1-weighed TSE MR images (**C**) and MRI signal intensity plots (**D**) of the cellular uptake of Gd_2O_3-based nanoprobes by PC-3 cells.

Notes: (**A**) FI fluorescence (green), excited by green light, is shown in the left panel. DAPI counterstained nuclei (blue), excited by blue light, are shown in the middle panel. Color overlays of green and blue fluorescence are shown in the right panel. *$P<0.05$.

Abbreviations: BBN, bombesin; FI, 5(6)-carboxyfluorescein; Gd_2O_3, gadolinium oxide; MRI, magnetic resonance imaging; PEG, polyethylene glycol; SNR, signal-to-noise ratio; TSE, turbo spin-echo.

controls. This indicated that the addition of BBN peptide to the NPs enhanced NP uptakes.

In vitro cellular MRI

The enhanced cellular uptake of the targeted nanoprobe was further confirmed by T1-weighted MRI in vitro. Figure 4C and D show that the T1 signal intensity of PC-3 cells incubated with Gd_2O_3-FI-PEG-BBN increased according to Gd concentrations. These MRI results further demonstrated

that surface functionalization by BBN enhanced the cellular uptake efficacy of NPs by specifically binding to overexpressed GRPR in cancer cells.[22]

In vivo MRI

To investigate the tumor targeting ability of the developed nanoprobe in vivo, serial T1-weighted images of PC-3 tumor-bearing mice were acquired before and at different time points after intravenous injection of Gd_2O_3-FI-PEG-BBN

or Gd₂O₃-FI-PEG. As shown in Figure 5A, the targeted Gd₂O₃-FI-PEG-BBN reached a peak MRI signal intensity 2 h postinjection and showed more obvious and prolonged signal enhancement in the tumor than the non-targeted probe after injection. MRI signal intensities of PC-3 tumors before and 2 h after injection were measured and plotted in Figure 5B

for quantitative analysis. The targeted nanoprobe resulted in a higher enhancement ratio than the non-targeted probe (27.9%±5.9% versus 4.0%±2.2%, respectively, $P<0.05$). According to our in vivo MRI results, the targeted Gd₂O₃-FI-PEG-BBN nanoprobe accumulated in cancerous tissues through the enhanced permeation and retention effect and
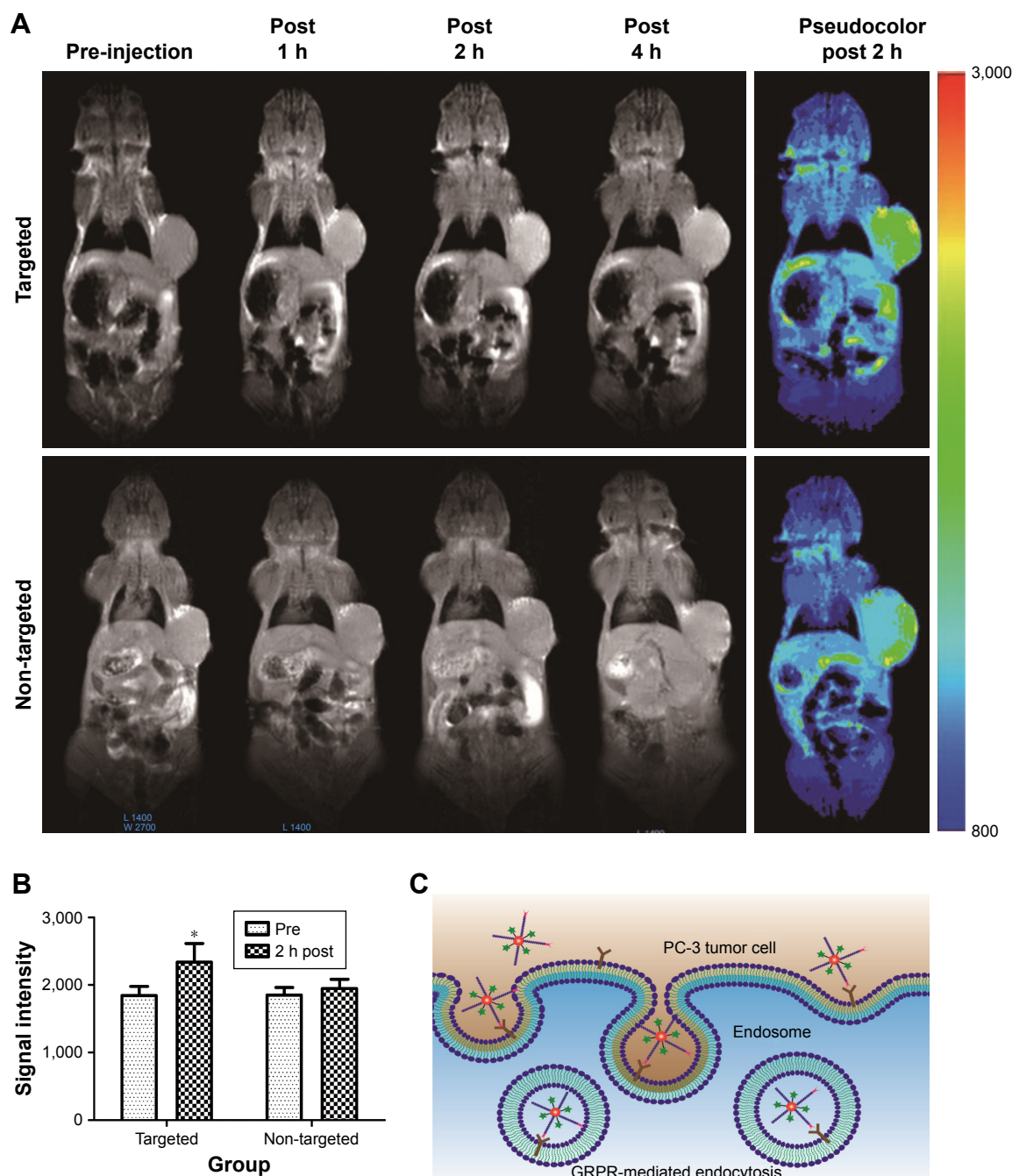
Figure 5 In vivo MR imaging.
Notes: Representative in vivo serial T1-weighted MR images (**A**) before and at 1, 2, and 4 h postinjection of targeted Gd₂O₃-FI-PEG-BBN or non-targeted Gd₂O₃-FI-PEG and pseudocolor maps of MR images 2 h after administering each agent. Quantitative analysis of signal intensity in the tumor region (**B**) of PC-3 tumor-bearing mice before and 2 h after intravenous injection. Schematic representation (**C**) of GRPR-mediated intracellular delivery. *$P<0.05$.
Abbreviations: BBN, bombesin; FI, 5(6)-carboxyfluorescein; Gd₂O₃, gadolinium oxide; GRPR, gastrin-releasing peptide receptor; MR, magnetic resonance; PEG, polyethylene glycol.

exhibited active targeting ability and selectively accumulated in the tumor sites (Figure 5C), which achieved the maximal contrast enhancement.[23]

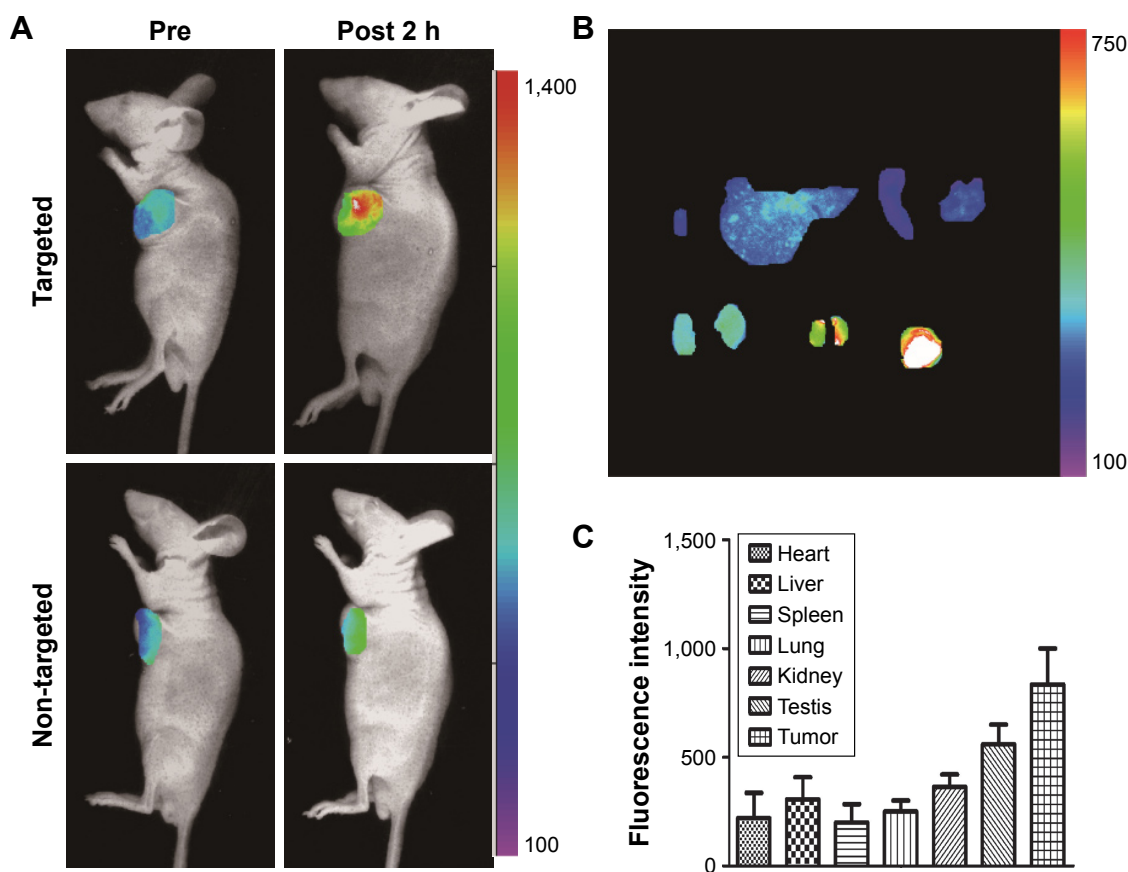## In vivo fluorescent imaging and biodistribution

The fluorescence intensity in tumors from the Gd_2O_3-FI-PEG-BBN nanoprobe was substantially greater than that in the non-targeted group, which indicated highly specific targeting of the Gd_2O_3-FI-PEG-BBN nanoprobe to PC-3 tumors (Figure 6A). As illustrated in Figure 6B, the NPs primarily accumulated in tumors. Significant fluorescence signal was also observed in the liver, spleen, lung, kidney and testis (Figure 6C), similar to the in vivo behaviors of many other nanomaterials applied in biomedicine.[24,25] Conversely, the nonspecific fluorescence distribution might be due to fluorescein dissociation from the nanoprobe. Therefore, the long-term fate of Gd_2O_3-FI-PEG-BBN requires further investigation.

Histological studies

Ex vivo fluorescence microscopy was used to further verify the accumulation of the developed nanoprobe in tumors. As shown in Figure 7, abundant green fluorescence was seen in tumor tissues after injecting Gd_2O_3-FI-PEG-BBN, but only a little green fluorescence was observed in the non-targeted group. This result demonstrated increased accumulation of targeted Gd_2O_3-FI-PEG-BBN in tumors that exhibited clear MRI contrast.[26] These results further confirmed the GRPR tumor-specific uptake of the targeted nanoprobe.

Conclusion

In summary, we have synthesized a BBN-modified Gd_2O_3-based nanoprobe with relatively good water dispersibility and favorable biocompatibility. PEG coating allowed modification with BBN ligand, which ensured the selective PC-3 cellular uptake, thus paving a way toward targeted delivery to PC tissues and the visualization of its accumulation by in vitro and in vivo MRI/fluorescent imaging. These multifunctional

Figure 6 In vivo fluorescent imaging and biodistribution.
Notes: In vivo optical images (**A**) of nude mice bearing subcutaneous PC-3 tumor xenografts after intravenous injection of Gd_2O_3-FI-PEG-BBN or Gd_2O_3-FI-PEG. Ex vivo fluorescence images (**B**) of dissected organs from mice bearing PC-3 tumors sacrificed after injecting Gd_2O_3-FI-PEG-BBN. Quantitative fluorescent intensities of isolated tumors and main organs (**C**).
Abbreviations: BBN, bombesin; FI, 5(6)-carboxyfluorescein; Gd_2O_3, gadolinium oxide; PEG, polyethylene glycol.
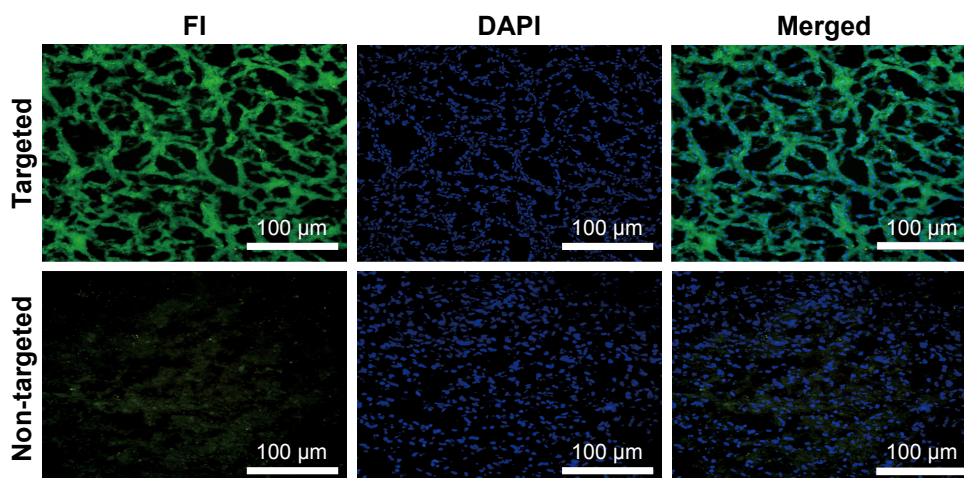
Figure 7 Fluorescence microscopy images of tumor tissues after intravenously injecting targeted Gd$_2$O$_3$-Fl-PEG-BBN or non-targeted Gd$_2$O$_3$-Fl-PEG.
Abbreviations: BBN, bombesin; Fl, 5(6)-carboxyfluorescein; Gd$_2$O$_3$, gadolinium oxide; PEG, polyethylene glycol.

Gd$_2$O$_3$-based NPs may be a potential nanoplatform for combined molecular cancer diagnosis and targeted antitumor drug delivery in future clinical applications.

Disclosure

The authors report no conflicts of interest in this work.

References

1. Siegel RL, Miller KD, Jemal A. Cancer statistics, 2017. *CA Cancer J Clin*. 2017;67(1):7–30.
2. Wolf AM, Wender RC, Etzioni RB, et al; American Cancer Society Prostate Cancer Advisory Committee. American Cancer Society guideline for the early detection of prostate cancer: update 2010. *CA Cancer J Clin*. 2010;60(2):70–98.
3. Woodrum DA, Kawashima A, Gorny KR, Mynderse LA. Prostate cancer: state of the art imaging and focal treatment. *Clin Radiol*. 2017; 72(8):665–679.
4. Beer M, Montani M, Gerhardt J, et al. Profiling gastrin-releasing peptide receptor in prostate tissues: clinical implications and molecular correlates. *Prostate*. 2012;72(3):318–325.
5. Wieser G, Mansi R, Grosu AL, et al. Positron emission tomography (PET) imaging of prostate cancer with a gastrin releasing peptide receptor antagonist – from mice to men. *Theranostics*. 2014;4(4):412–419.
6. Zhang J, Niu G, Lang L, et al. Clinical Translation of a dual integrin alphavbeta3- and gastrin-releasing peptide receptor-targeting PET radiotracer, 68Ga-BBN-RGD. *J Nucl Med*. 2017;58(2):228–234.
7. Lim JC, Cho EH, Kim JJ, et al. Preclinical pharmacokinetic, biodistribution, imaging and therapeutic efficacy of (177)Lu-labeled glycated bombesin analogue for gastrin-releasing peptide receptor-positive prostate tumor targeting. *Nucl Med Biol*. 2015;42(3):234–241.
8. Richter S, Wuest M, Krieger SS, et al. Synthesis and radiopharmacological evaluation of a high-affinity and metabolically stabilized 18F-labeled bombesin analogue for molecular imaging of gastrin-releasing peptide receptor-expressing prostate cancer. *Nucl Med Biol*. 2013; 40(8):1025–1034.
9. Liang J, Zhang X, Miao Y, Li J, Gan Y. Lipid-coated iron oxide nanoparticles for dual-modal imaging of hepatocellular carcinoma. *Int J Nanomedicine*. 2017;12:2033–2044.
10. Ni K, Zhao Z, Zhang Z, et al. Geometrically confined ultrasmall gadolinium oxide nanoparticles boost the T(1) contrast ability. *Nanoscale*. 2016;8(6):3768–3774.
11. Liu J, Huang L, Tian X, et al. Magnetic and fluorescent Gd2O3:Yb3+/Ln3+ nanoparticles for simultaneous upconversion luminescence/MR dual modal imaging and NIR-induced photodynamic therapy. *Int J Nanomedicine*. 2017;12:1–14.
12. Han L, Xia JM, Hai X, Shu Y, Chen XW, Wang JH. Protein-stabilized gadolinium oxide-gold nanoclusters hybrid for multimodal imaging and drug delivery. *ACS Appl Mater Interfaces*. 2017;9(8):6941–6949.
13. Steinmetz NF, Ablack AL, Hickey JL, et al. Intravital imaging of human prostate cancer using viral nanoparticles targeted to gastrin-releasing peptide receptors. *Small*. 2011;7(12):1664–1672.
14. Hu Z, Ahren M, Selegard L, et al. Highly water-dispersible surface-modified Gd(2)O(3);nanoparticles for potential dual-modal bioimaging. *Chemistry*. 2013;19(38):12658–12667.
15. Nan X, Zhang X, Liu Y, Zhou M, Chen X, Zhang X. Dual-targeted multifunctional nanoparticles for magnetic resonance imaging guided cancer diagnosis and therapy. *ACS Appl Mater Interfaces*. 2017;9(11): 9986–9995.
16. Xia Y, Wang Y, Wang Y, et al. A tumor pH-responsive complex: carboxyl-modified hyperbranched polyether and cis-dichlorodiammineplatinum(II). *Colloids Surf B Biointerfaces*. 2011;88(2): 674–681.
17. Gong H, Dong ZL, Liu YM, et al. Engineering of multifunctional nano-micelles for combined photothermal and photodynamic therapy under the guidance of multimodal imaging. *Adv Funct Mater*. 2014; 24(41):6492–6502.
18. Anishur RA, Majewski P, Vasilev K. Gd2O3 nanoparticles: size-dependent nuclear magnetic resonance. *Contrast Media Mol Imaging*. 2013;8(1):92–95.
19. Wang F, Peng E, Liu F, Li P, Li SF, Xue JM. Fluorescence-tagged amphiphilic brush copolymer encapsulated Gd2O3 core-shell nanostructures for enhanced T1 contrast effect and fluorescent imaging. *Nanotechnology*. 2016;27(42):425101.

20. Kumar S, Meena VK, Hazari PP, Sharma RK. FITC-Dextran entrapped and silica coated gadolinium oxide nanoparticles for synchronous optical and magnetic resonance imaging applications. *Int J Pharm*. 2016; 506(1–2):242–252.

21. Pan D, Yan Y, Yang R, et al. PET imaging of prostate tumors with 18F-Al-NOTA-MATBBN. *Contrast Media Mol Imaging*. 2014;9(5): 342–348.

22. Chen H, Wan S, Zhu F, et al. A fast tumor-targeting near-infrared fluorescent probe based on bombesin analog for in vivo tumor imaging. *Contrast Media Mol Imaging*. 2014;9(2):122–134.

23. Jia Z, Song L, Zang F, et al. Active-target T1-weighted MR imaging of tiny hepatic tumor via RGD modified ultra-small Fe_3O_4 nanoprobes. *Theranostics*. 2016;6(11):1780–1791.

24. Lin YH, Dayananda K, Chen CY, et al. In vivo MR/optical imaging for gastrin releasing peptide receptor of prostate cancer tumor using Gd-TTDA-NP-BN-Cy5.5. *Bioorg Med Chem*. 2011;19(3):1085–1096.

25. Naccache R, Chevallier P, Lagueux J, et al. High relaxivities and strong vascular signal enhancement for NaGdF4 nanoparticles designed for dual MR/optical imaging. *Adv Healthc Mater*. 2013;2(11):1478–1488.

26. Zhou Z, Han Z, Lu ZR. A targeted nanoglobular contrast agent from host-guest self-assembly for MR cancer molecular imaging. *Biomaterials*. 2016;85:168–179.